Transactions of the SMiRT 27
Yokohama, Japan, March 3-8, 2024
Division XII

INVESTIGATION OF THE ROBUSTNESS OF THE PBF-LB/M PROCESS FOR AISI 316L IN CONTEXT OF SAFETY-CRITICAL COMPONENTS FOR NUCLEAR APPLICATIONS

Sven Sewalski[1], Martin Werz[2], Stefan Weihe[3]

[1] Scientific Associate, Materials Testing Institute (MPA) University of Stuttgart, Stuttgart, Germany (sven.sewalski@mpa.uni-stuttgart.de)
[2] Head of Department Joining Technology and Additive Manufacturing, Materials Testing Institute (MPA) University of Stuttgart, Stuttgart, Germany
[3] Professor, Materials Testing Institute (MPA) University of Stuttgart, Stuttgart, Germany

ABSTRACT

In the future, additive manufacturing processes will play an important role in the production of modern reactor concepts such as SMRs as well as in the manufacturing of spare parts for existing nuclear power plants. In nuclear applications, the requirements for the components are particularly high. Therefore, the robustness of the PBF-LB/M process for the austenitic stainless steel AISI 316L in the context of safety-critical components is experimentally investigated in this study. For this purpose, the susceptibility of the process to disturbances as well as their impact on the microstructure and mechanical properties of additively manufactured AISI 316L is analysed. The experimental results allow an assessment of whether the PBF-LB/M process can be used to reliably manufacture safety-critical components for nuclear applications.

INTRODUCTION

Additive manufacturing processes such as powder bed fusion of metals with laser beam (PBF-LB/M) are being considered for the production of components for modern reactor concepts such as small modular reactors (SMR) (Lou2019). The PBF-LB/M process allows the designer a very high degree of design freedom due to the layer-by-layer build up process, which means that geometries can be realized that cannot be manufactured using conventional processes such as forming, turning or milling. In addition, through functional integration, entire assemblies can be replaced by a single additively manufactured component, which can save costs. The quality requirements for components are particularly high in nuclear applications. In order to meet these high requirements, precise knowledge of how the individual process parameters of the PBF-LB/M influence the microstructure and the mechanical properties is required. The PBF-LB/M process is characterized by a great number of parameters that influence the process results and thus, the quality of the manufactured components. The most important process parameters here are the laser power P, the scanning speed v, the hatch distance h as well as the layer thickness t_L (Keshavarzkermani2019). However, parameters such as the build plate temperature T_0, the flow velocity of the inert gas circulation, the laser beam diameter d_B and the properties of the powder material (e.g. the moisture content) also play an important role. Further, the robustness of the process is characterized by the microstructure as well as by the mechanical-technological properties and the relative density of the molten and then solidified powder in each layer.

Austenitic stainless steels such as AISI 316L are widely used for existing Generation III reactors and are a promising material candidate for future Generation IV reactors due to their excellent corrosion resistance and good mechanical properties at the operating temperatures and pressures (Puichaud2019). Therefore, various series of experiments analyzing the effect of the process parameters laser power P, scanning speed v, hatch distance h and the laser beam diameter d_B on the microstructure and the mechanical properties of AISI 316L are being carried out in this work. The extent to which the respective process parameters can be varied without significantly changing the process result is investigated. In the investigation of the microstructure, the grain sizes and their orientations, the dimensions of the melt pools and the morphology of the dendritic solidification structures are considered. The hardness, ultimate tensile strength and relative component density are examined to determine the mechanical-technological material properties. The results are used to assess the robustness of the PBF-LB/M process regarding the manufacturing of safety-relevant nuclear components, such as liquid metal heat pipes which are used in some SMR concepts, with the material AISI 316L.

MATERIALS AND METHODS

AISI 316L Metal Powder

The alloy AISI 316L (X2CrNiMo17-12-2, DIN 1.4404) has good weldability and is therefore frequently used in PBF-LB/M (Ma2017). AISI 316L is a stainless, austenitic chromium-nickel-molybdenum steel with a low carbon content. The very good corrosion resistance of AISI 316L can be attributed to the high chromium content of more than 16 wt.%, which forms a chromium-rich, passivating oxide layer on the surface (Diaz2021). Table 1 shows the limits for the chemical composition of AISI 316L according to ASTM A276. Additively manufactured components made of AISI 316L have a higher corrosion resistance compared to conventionally manufactured products (Chao2017). This is due to the fact that there are no MnS inclusions in additively manufactured AISI 316L, which play a role in the initiation of pitting corrosion (Ryan2002). Studies regarding MnS inclusions proofed that various nanoscale inclusions containing Mn and S are being induced by the PBF-LB/M process (Vukkum2022).

AISI 316L metal powder from the manufacturer m4p materials solution GmbH is used to manufacture the sample material. The particle size fraction is in the range of 15-45 µm. The percentages of the respective alloying elements are within the range specified by ASTM A276, refer to Table 1.

Table 1: Chemical composition in wt.% of AISI 316L according to ASTM A276 and chemical composition of the metal powder used in this study.

	C	Si	Mn	Cr	Mo	Ni	Fe
min.	-	-	-	16.00	2.00	10.00	balance
max.	0.030	0.75	2.00	18.00	3.00	14.00	balance
metal powder used	0.025	0.61	1.34	17.00	2.15	10.90	balance

PBF-LB/M-System

The modular "Evobeam SLaVAM 300" system from the manufacturer Evobeam GmbH, which is located at the Materials Testing Institute (MPA) University of Stuttgart, is used to produce the additively manufactured sample material. The TruFiber 2000 laser integrated into the system enables an adjustable laser power of 60 W - 2000 W at a wavelength of λ = 1075 ± 7 nm.

Samples

Different sample types are used to characterize the influence of process parameters on the mechanical properties of additively manufactured AISI 316L. Sample cubes with an edge length of 8 mm are used to determine the relative density and to create metallographic micrographs. The 18 selected parameter sets analysed in this study are given in Table 2. Tensile specimens according to DIN 50125 A 6 x 30 are used to determine the yield and tensile strength. They are manufactured in an upright position so that the load is applied along the build direction during the tensile tests. No post-processing steps are performed since this study focuses on the mechanical properties of as-printed material.

Sample Manufacturing by PBF-LB/M

The samples are manufactured in two separate build jobs. In build job I, for each of the 18 parameter sets one test cube is manufactured. The tensile specimens are printed in build job II. Here, three tensile specimens are provided for selected parameter sets to consider scattering of the material properties. The digital process preparation is carried out with the 3D printing software Autodesk Netfabb®. The scan strategy selected is "lines" and the tilt angle of the scan paths of the subsequent layer is set to 67°. Argon is used as the inert gas for both build jobs.

Table 2 shows an overview of all selected process parameter sets. The individual parameters were varied in such a way that a reasonably high relative density was achieved for all parameter sets. The experiments for determining the influences of the PBF-LB/M process parameters are designed using the DOE method OFAT (one factor at a time). By varying subsequently each parameter of parameter set 3, the influence of the laser power P (1-5), the scanning speed v (6-9), the hatch distance h (10-14) and the laser beam diameter d_B (15-18) are investigated in four series of experiments. The volume energy density *VED* was calculated for all parameter sets and is shown in Table 2.

Table 2: Process parameters and corresponding relative densities and *PDAS* achieved with them.

No.	**P**	**v**	**h**	**d_B**	**t_L**	**T_0**	**VED**	**Relative density**	**PDAS**
	W	m/s	µm	µm	µm	°C	J/mm³	%	µm
1	142	0.68	80	62	30	200	87.00	99.93	0.56 ± 0.05
2	180						110.3	99.98	0.59 ± 0.04
3	218						133.6	99.99	0.60 ± 0.05
4	256						156.9	99.99	0.66 ± 0.06
5	294						180.1	99.97	0.75 ± 0.10
6	218	0.40	80	62			227.1	99.98	0.72 ± 0.12
7		0.54					168.2	99.99	0.71 ± 0.06
8		0.82					110.7	99.97	0.61 ± 0.05
9		0.96					94.62	99.85	0.64 ± 0.04
10	218	0.68	50	62			213.7	99.98	0.75 ± 0.06
11			60				178.1	99.99	0.64 ± 0.02
12			70				152.7	99.96	0.67 ± 0.04
13			90				118.7	99.99	0.66 ± 0.06
14			100				106.9	99.97	0.62 ± 0.05
15	218	0.68	80	63			133.6	99.98	0.65 ± 0.10
16				70			133.6	99.98	0.66 ± 0.07
17				80			133.6	99.52	0.66 ± 0.07
18				90			133.6	99.84	0.70 ± 0.07

Metallography

To create the micrographs, the sample cubes are hot-mounted at approx. 200 °C, grinded, polished and then vibratory polished with an ultra-fine polishing suspension (0.05 µm particles). The grinding plane is located in the center of each sample cube and aligns with the build direction. The microsections are electrolytically etched with a 10% oxalic acid solution for 120 s - 180 s to evaluate the microstructure. The microstructure of the individual samples is determined by the size and orientation of the individual grains, the melt pool dimensions, the overlap of the melt pools and the size of the dendritic structures. The density is determined for all 18 sample cubes by optical image analysis of the polished sections.

For this purpose, nine images with a 200x magnification are taken for each section so that even small pores (> 0.5 µm) can be included in the density analysis.

Determining Mechanical Properties

The hardness tests in accordance with DIN EN ISO 6507-1:2018-07 are carried out using the Zwick Z 323 testing device from ZwickRoell. For each sample cube, nine measurements are carried out in a 3x3 grid on the microsection plane. The hardness values of the 18 samples have a constant hardness level of 221 ± 4 HV1. All tensile tests are carried out using the ZwickRoell BZ1 tensile testing machine (maximum tensile force: 100 kN). The parameters of the test specification are set in accordance with test method B to DIN EN ISO 6892-1. The yield and tensile strength of the three tensile tests are averaged for each parameter set and the standard deviation is calculated to indicate the scattering behaviour of the measured values.

RESULTS

Figure 1 shows representative micrographs for all 18 sample cubes. All of the 18 samples have a high relative density of > 99.5 % and 15 of the 18 samples have a density of greater than 99.9 %. In order to obtain information on the phase composition of the individual parameter sets, the fraction of magnetic phases is measured with a ferrite detector. Each sample is measured at nine points with the detector, showing a value of 0.00 % for all measurements. Consequently, no magnetic phase components such as delta ferrite or martensite are present in the sample material and it can be assumed that a completely austenitic microstructure is present in all samples. To determine the melt pool width b_s and melt pool depth t_s, at least six individual melt pools of the uppermost layer are measured for each sample. The solidification morphology is cellular dendritic for all of the 18 sample cubes. The primary dendritic arm spacing (*PDAS*) is determined by measuring five dendritic colonies in each case. A 20 µm long line is placed in each colony and the number of dendrites intersecting this line is counted. In order to obtain a representative *PDAS* for the respective sample, the mean *PDAS* of the five colonies under consideration are arithmetically averaged. For all 18 parameter sets, the measured *PDAS* for individual dendrite colonies lies within a value range of 0.48 µm - 1.18 µm. The majority of the samples have a mean *PDAS* between 0.56 µm and 0.75 µm, which is consistent with literature data (Diaz2021, Kong2020, Pham2020, Krakhmalev2018).

The different process parameter sets cause visible differences in the microstructures. Figure 2 shows the influence of the laser power on the grain structure. The grain structure is characterized by elongated grains along the build-up direction. When a low power of 142 W is used, a fine grain structure is formed, whereby the aspect ratio of the grains is relatively low. Higher power levels such as 218 W and 294 W favor the growth of larger grains along the build-up direction, some of which extend over more than 15 layers.

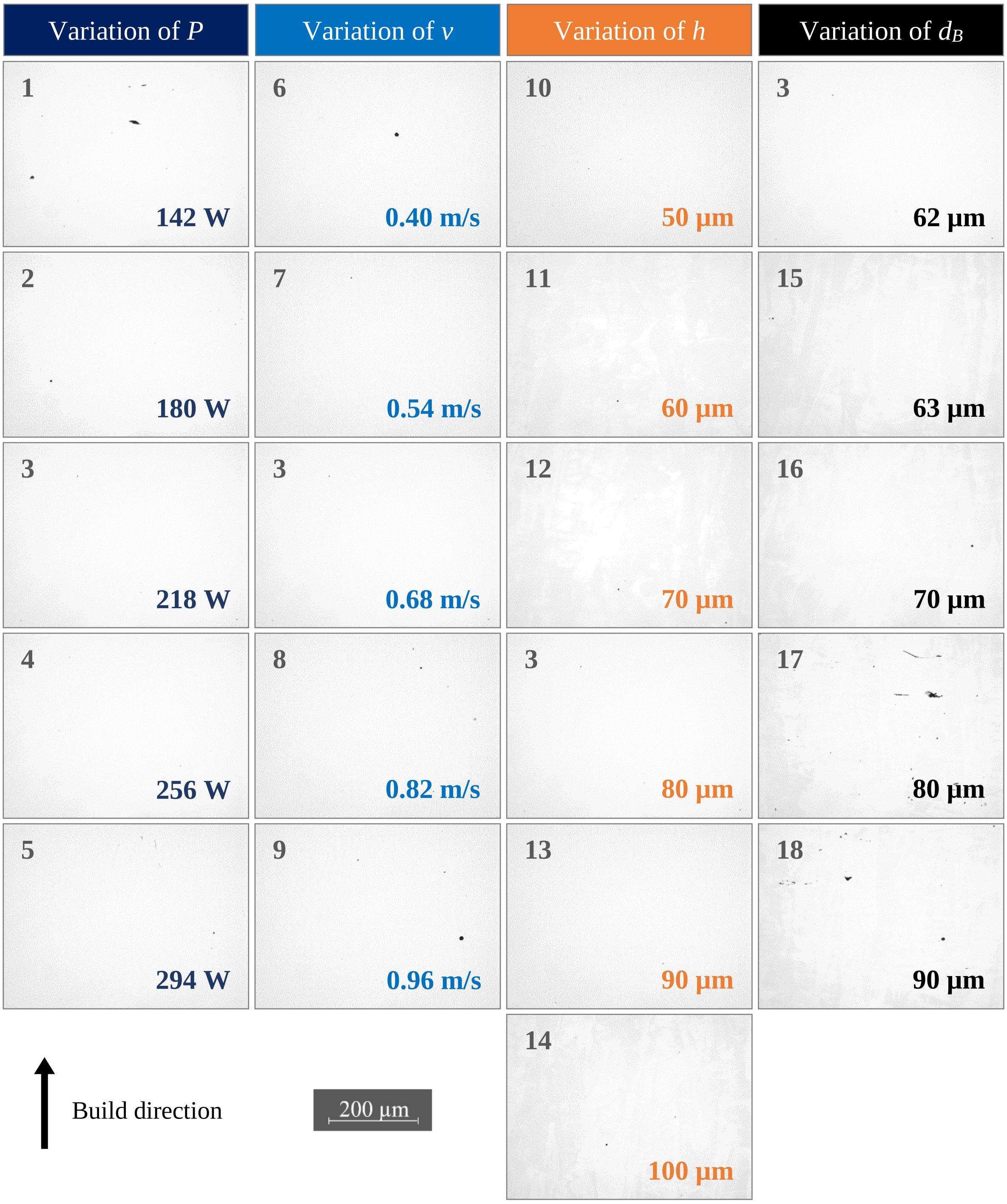

Figure 1. Polished micrographs for the analyzed parameter sets 1-18, a representative micrograph is shown for each sample cube. The variations of the process parameters P, v, h and d_B are shown in columns.

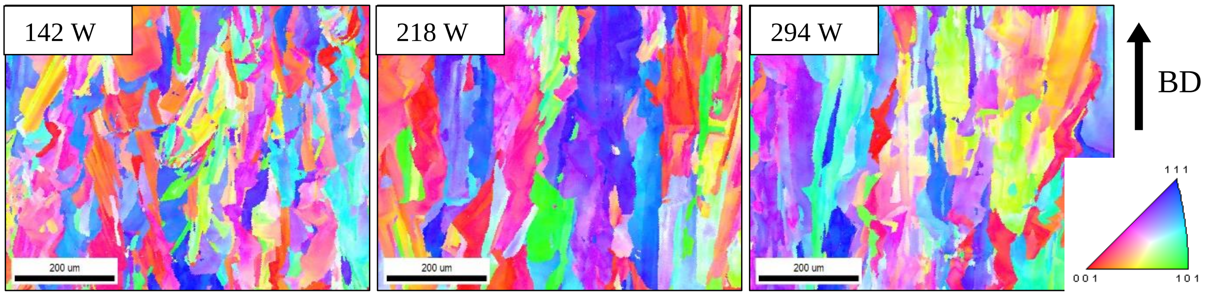

Figure 2. EBSD images for P = 142, 218, 294 W at v = 0.68 m/s, h = 80 µm and d_B = 62 µm with BD representing the build direction.

Influence of the Process Parameters on the Material Properties

In figure 3, the influences of the process parameters laser power P, scanning speed v, hatch distance h and laser beam diameter d_B on the mechanical properties are shown. With increasing laser power, both the ultimate tensile strength UTS and the yield strength YS decrease within the investigated range. When the power is increased from 142 W to 294 W, UTS is reduced from 564 MPa to 520 MPa and YS from 469 MPa to 405 MPa. The hardness is not statistically significantly influenced by the laser power within the scope of the varied power and is at a constant level of 221 ± 4 HV1.

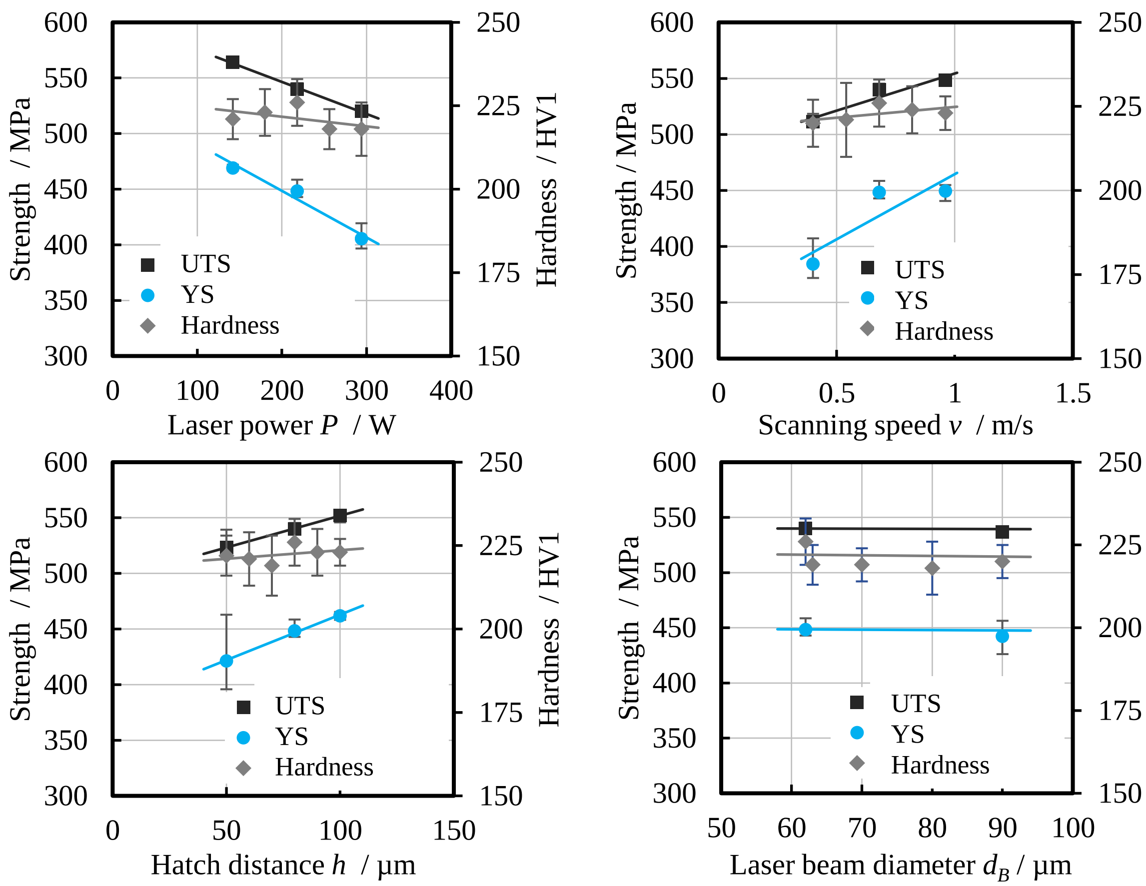

Figure 3. Influence of the process parameters P, v, h and d_B on the strength and hardness. For each series of tests, only the process parameter under consideration was varied.

The strength parameters YS and UTS correlate with the scanning speed within the examined range. At scanning speed of v = 0.4 m/s, the yield strength YS equals 384 MPa and the ultimate tensile strength UTS equals 511 MPa. By increasing the scanning speed to 0.96 m/s, YS is increased to

449 MPa and UTS to 548 MPa. The influence of the scanning speed on the strength is slightly lower than the influence caused by the laser power in relation to the respective investigated interval, as the scanning speed was increased by 140 % and the laser power by 107 % within the test series. As with the laser power, the hardness of the material is not significantly influenced by the scanning speed.

The hatch distance is doubled from 50 µm to 100 µm and has a similar effect as the scanning speed on the strength and hardness. The correlation is apparent with a variation of the hatch distance from 50 µm to 100 µm through the increase of YS from 421 MPa to 462 MPa and of UTS from 524 MPa to 552 MPa. The influence of the hatch distance on the strength is therefore less than that of the scanning speed. As with the laser power and the scanning speed, the influence on the strength does not correlate with the hardness, as this is not significantly influenced by the variation in the process parameters.

The strength and hardness are virtually unaffected by an increase in the laser beam diameter d_B. The tensile strength is reduced by increasing the laser beam diameter by a factor of 1.45 from 540 MPa to 537 MPa and the yield strength from 448 MPa to 442 MPa.

The influence of the linear energy density *LED* (*LED* = *P/v*) on the primary dendrite arm spacing is shown in Figure 4. The data determined in this study is supplemented by data from Kong et al. (Kong2020). For low *LED*s of less than 0.1 J/mm, *PDAS* of less than 0.5 µm are achieved. Linear energy densities in the range of 0.1 J/mm - 0.55 J/mm lead to *PDAS* of 0.55 µm - 0.77 µm, which is in agreement with literature data (Pham2020, Krakhmalev2018, Mertens2014). A further increase of the linear energy density up to 2 J/mm leads to *PDAS* of up to 0.98 µm. The power function in Figure 4, approximated by least squares error, describes the relationship between *LED* and *PDAS* and shows good agreement with the measured values. Kong et al. were able to obtain an average *PDAS* of 1.2 µm with the process parameters P = 195 W, v = 0.25 m/s, h = 200 µm and t_L = 20 µm (Kong2020). However, the relative density of the samples was not specified.

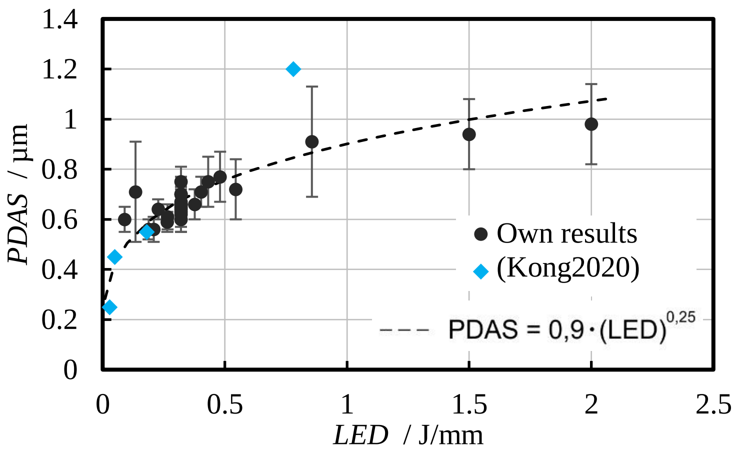

Figure 4. Influence of the linear energy density *LED* on primary dendritic arm spacing *PDAS* for AISI 316L.

Figure 5 shows the influence of the process parameters P, v, h and d_B on the melt pool width and depth as well as on the primary dendrite arm spacing. As the laser power increases, the melt pools become wider and deeper, as more energy is provided for melting the material. The increased energy input due to the increasing power reduces the cooling rate $\dot{T}$, resulting in a coarser microstructure. The *PDAS* is increased from 0.55 µm at 142 W to 0.75 µm at 294 W.

Increasing the scanning speed leads to a reduction in the melt pool width and depth and a decrease in the primary dendrite arm spacing. An increase in v therefore has a similar effect as a reduction in P, as this reduces the energy input into the process. The melt pool widths and depths achieved with v = 0.4 m/s are disproportionately large compared to those with higher values for v. This may indicate that a small near-surface keyhole has led to increased energy input. When looking at the melt pool dimensions, no clear tendency can be observed for the influence of the hatch distance, as the measured values scatter. The *PDAS* also show a high scatter, but the *PDAS* tends to decrease with increasing *h* from 0.74 µm at $h = 50$ µm to 0.62 µm at $h = 100$ µm. Increasing the laser beam diameter causes a decrease in the weld penetration depth with a simultaneous increase in the weld pool width and the *PDAS*. The increase in d_B reduces the intensity of the laser radiation, which explains the changes in the weld pool dimensions. The increase in PDAS could be explained by the fact that the laser beam has a longer exposure time to each point in its path due to the larger laser beam diameter, thus reducing the cooling rate.

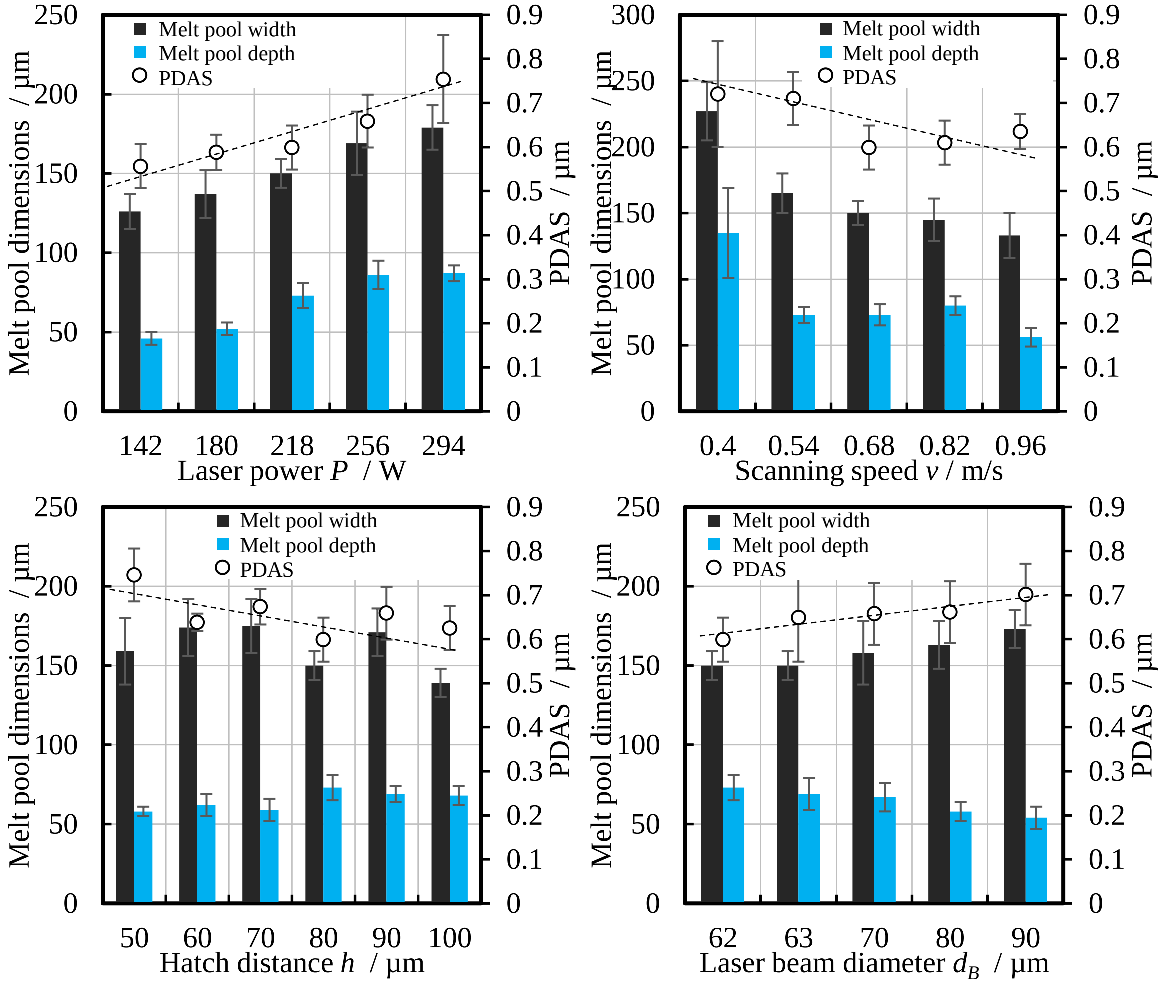

Figure 5. Influence of the process parameters *P*, *v*, *h* and d_B on the melt pool dimensions and *PDAS*. For each test series, only the process parameter under consideration was varied.

DISCUSSION

The process parameters *P*, *v*, *h* and d_B were varied in four series of tests, whereby the direct influences on the mechanical properties and the microstructure were identified. The tensile strength could be influenced in a range of 511 MPa – 564 MPa, which corresponds to a relative influence of 10 %. The hardness of all samples could not be significantly influenced by the different process conditions and is in the range of 221 ± 4 HV1 for all tested samples. It is noticeable that the tensile strength was clearly influenced by the different process parameters, while the hardness was not significantly changed. Possible explanations for this behaviour could lie in the anisotropy of the microstructure or in an asymmetric tension-compression behaviour. The fact that the mechanical properties can be influenced only slightly by varying the process parameters means that the PBF-LB/M process for AISI 316L is robust with regard to the heat input resulting from different process parameters. In contrast, (Großwendt2021) showed that changing the chemical composition within the specified range for AISI 316L in ASTM A276 influences the tensile strength by 34 % and hardness by 27 %. This indicates that the mechanical properties are influenced more by the chemical composition than by the process (solidification, heat input, …) itself. By varying the process parameters, the melt pool width and depth can be specifically adjusted. The solidification conditions of the melt can also be adjusted by the process parameters, resulting in different dendrite arm spacings. In this study, however, the dendrite arm spacing could only be varied in a range of 0.55 µm - 0.98 µm. By varying the process parameters, the size and aspect ratio of the grains can also be influenced. Modern scanning strategies can include different process parameter combinations, which is why the same component can contain local differences in the grain structure. In the context of safety-relevant components that are subjected to high stresses at high temperatures, these differences in the microstructure can, for example, potentially affect the creep damage progression.

CONCLUSION

The experimental investigations in this study were used to describe the influences of the process parameters on the material properties and microstructure of additively manufactured AISI 316L. The following conclusions can be drawn from the results of this study:

- Robust process parameter sets exist for AISI 316L material that can achieve high relative densities even when individual process parameters are varied within a wide range
- The cellular morphology of the dendritic solidification structure is stable even when the process parameters are varied and the size of the dendrite arm spacing is in the range of 0.56 - 0.75 µm
- The size and aspect ratio of the grains depend on the process parameters
- The hardness of AISI 316L for sample material with a relative density > 99.9 % cannot be significantly influenced by the process parameters
- The mechanical properties of AISI 316L can be influenced more by the chemical composition than by changing the process parameters
- Further investigations are necessary to clarify why the variation of the process parameters has a noticeable effect on the tensile strength, whereas the hardness remains almost unaffected

REFERENCES

Chao, Q., Cruz, V., Thomas, S., Birbilis, N., Collins, P., Taylor, A., ... & Fabijanic, D. (2017). “On the enhanced corrosion resistance of a selective laser melted austenitic stainless steel”. Scripta Materialia, 141, 94-98.

Diaz Vallejo, N., Lucas, C., Ayers, N., Graydon, K., Hyer, H., & Sohn, Y. (2021). “Process optimization and microstructure analysis to understand laser powder bed fusion of 316l stainless steel”. Metals, 11(5), 832.

Großwendt, F., Becker, L., Röttger, A., Chehreh, A. B., Strauch, A. L., Uhlenwinkel, V., ... & Theisen, W. (2021). “Impact of the allowed compositional range of additively manufactured 316L stainless steel on processability and material properties”. Materials, 14(15), 4074.

Keshavarzkermani, A., Marzbanrad, E., Esmaeilizadeh, R., Mahmoodkhani, Y., Ali, U., Enrique, P. D., ... & Toyserkani, E. (2019). “An investigation into the effect of process parameters on melt pool geometry, cell spacing, and grain refinement during laser powder bed fusion”. Optics & Laser Technology, 116, 83-91.

Kong, D., Dong, C., Ni, X., Zhang, L., & Li, X. (2020). „Cellular size dependence on the strength of additively manufactured austenitic stainless steel”. Materials Letters, 279, 128524.

Krakhmalev, P., Fredriksson, G., Svensson, K., Yadroitsev, I., Yadroitsava, I., Thuvander, M., & Peng, R. (2018). “Microstructure, solidification texture, and thermal stability of 316 L stainless steel manufactured by laser powder bed fusion”. Metals, 8(8), 643.

Lou, X., & Gandy, D. (2019). “Advanced manufacturing for nuclear energy”. Jom, 71(8), 2834-2836.

Ma, M., Wang, Z., & Zeng, X. (2017). „A comparison on metallurgical behaviors of 316L stainless steel by selective laser melting and laser cladding deposition". Materials Science and Engineering: A, 685, 265-273.

Mertens, A., Reginster, S., Contrepois, Q., Dormal, T., Lemaire, O., & Lecomte-Beckers, J. (2014, June). "Microstructures and mechanical properties of stainless steel AISI 316L processed by selective laser melting". In Materials Science Forum (Vol. 783, pp. 898-903). Trans Tech Publications Ltd.

Pham, M. S., Dovgyy, B., Hooper, P. A., Gourlay, C. M., & Piglione, A. (2020). "The role of side-branching in microstructure development in laser powder-bed fusion". Nature communications, 11(1), 749.

Puichaud, A. H., Flament, C., Chniouel, A., Lomello, F., Rouesne, E., Giroux, P. F., ... & Béchade, J. L. (2019). "Microstructure and mechanical properties relationship of additively manufactured 316L stainless steel by selective laser melting". EPJ Nuclear Sciences & Technologies, 5, 23.

Ryan, M. P., Williams, D. E., Chater, R. J., Hutton, B. M., & McPhail, D. S. (2002). "Why stainless steel corrodes". Nature, 415(6873), 770-774.

Vukkum, V. B., & Gupta, R. K. (2022). „Review on corrosion performance of laser powder-bed fusion printed 316L stainless steel: Effect of processing parameters, manufacturing defects, post-processing, feedstock, and microstructure". Materials & Design, 110874.